ACS Photonics

pubs.acs.org/journal/apchd5

Article

Higher-Order Photon Statistics as a New Tool to Reveal Hidden Excited States in a Plasmonic Cavity

Philipp Stegmann,* Satyendra Nath Gupta, Gilad Haran, and Jianshu Cao

Cite This: https://doi.org/10.1021/acsphotonics.2c00375

Read Online

ACCESS | Metrics & More | Article Recommendations | Supporting Information

ABSTRACT: Among the best known quantities obtainable from photon correlation measurements are the $g^{(m)}$ correlation functions. Here, we introduce a new procedure to evaluate these correlation functions based on higher-order factorial cumulants $C_{F,m}$ that integrate over the time dependence of the correlation functions, that is, summarize the available information at different time spans. In a systematic manner, the information content of higher-order correlation functions as well as the distribution of photon waiting times is taken into account. Our procedure greatly enhances the sensitivity for probing correlations and, moreover, is robust against a limited counting efficiency and time resolution in experiment. It can be applied even in case $g^{(m)}$ is not accessible at short time spans. We use the new evaluation scheme to analyze the photon emission of a plasmonic cavity coupled to a single quantum dot. We derive criteria that must hold if the system can be described by a generic Jaynes−Cummings model. A violation of the criteria can be explained by the presence of an additional excited quantum dot state.

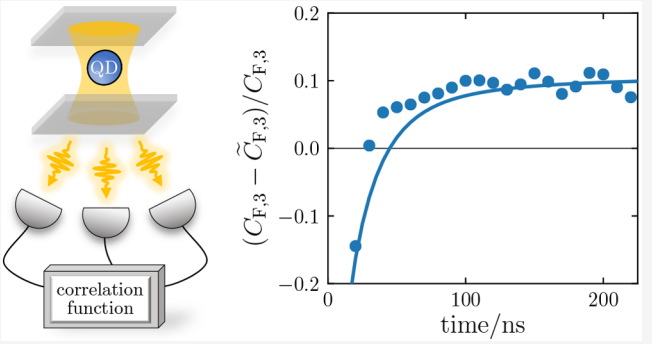

KEYWORDS: *photon statistics, correlation functions, plasmonic cavities, quantum dots, excitons, factorial cumulants*

Photon correlation functions are an important concept in the analysis of quantum optical systems.[1] The nature of the emitted light can be characterized conveniently by the second-order correlation function $g^{(2)}(t)$.[2] Classical description leads to $g^{(2)}(0) > 1$ for chaotic or thermal sources emitting photons in bunches.[3−5] In contrast, quantum emitters as single atoms or molecules[6−12] can give rise to $g^{(2)}(0) < 1$, indicating nonclassical light in form of an antibunched photon stream. Moreover, the value $g^{(2)}(0)$ can be used to verify the presence of quantum coherence[13] or to obtain the number of quantum emitters.[2,14−16]

Higher-order correlation functions $g^{(m)}$ provide a more precise characterization of photon statistics, which is a crucial requirement in the development of quantum technologies[17] and the engineering of single-photon emitters.[18] The third-order correlation function can be used to differentiate between the conventional and unconventional photon blockade effect.[11,19,20] Higher-order antibunching ($g^{(m)}(0) < 0$) can be identified[21−23] even though in second order the photon stream is bunched.[22−26] Universal relations between the different correlation functions have also been found for certain system classes.[16,21]

The analysis of correlation functions is typically focused on the limit of vanishing time delay $t = 0$. Though, finite-time correlations are measured as well, their interpretation is more challenging[2] and the complexity increases with each order. In this paper, we introduce a new procedure to evaluate the correlation functions systematically at finite times. The procedure is based on factorial cumulants $C_{F,m}$[27−30] and addresses certain experimental and theoretical issues. First, the evaluation is robust against a limited time resolution. Second, the counting efficiency of the measurement apparatus does not lead to systematic errors, that is, errors with a nonzero mean. A small efficiency can be compensated by increasing the measurement time and acquiring more data. Third, photon emitters can be distinguished systematically even in case $g^{(m)}$ is not accessible at short time delays. Fourth, we combine the information from the correlation functions with the concept of waiting times,[31,32] which provides complementary statistical insight.

The waiting-time distribution w between successive photon emission events can be constructed from all orders of the correlation functions $g^{(m)}$, but is also directly measurable in experiment.[33−35] The distribution characterizes photon bunching and antibunching in a more precise manner than the second-order correlation function.[5,36,37] Nevertheless, the

Received: March 7, 2022

difference between both quantities is small for times smaller than the average waiting time. Waiting times have been used frequently to study the statistics of electron currents in nanoscale junctions[38−50] and enzymatic reactions.[32,51−56] However, they have been used seldom in the analysis of single-photon emitters.[36,37]

In this paper, we follow the experimental work of Gupta et al.[66] and study the photon emission of a plasmonic cavity with an embedded quantum dot sketched in Figure 1a. Details

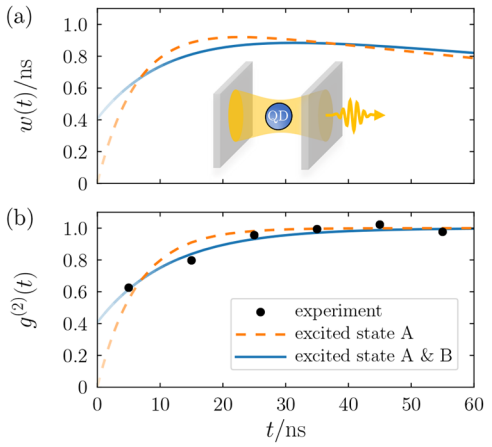

Figure 1. Photon emission statistics of a plasmonic cavity coupled to a single quantum dot. (a) Waiting-time distribution between consecutive photon counts. (b) Second-order correlation function. The experimental signal is binned in time intervals Δt = 10 ns (black dots). The parameters used for the simulation (solid blue and dashed orange curves) are given in Methods.

regarding the experimental setup are given in Methods. Plasmonic cavities have been investigated intensively in recent years for their ability to be strongly coupled to quantum emitters.[20,57−66] Here, the plasmonic cavity is made of a silver bowtie structure, and a single quantum dot is inserted in the gap at the center of the bowtie. Such systems have been described very successfully in literature by the well-known Jaynes−Cummings model,[67,68] where the dot is modeled as a two-level system with a ground and excited state A. The resulting waiting-time distribution $w(t)$ and second-order correlation function $g^{(2)}(t)$ are shown as dashed orange curves in Figure 1.

We will discuss how to identify deviations from this generic type of photon statistics due to the presence of a second excited state B (see solid blue curves) strongly coupled to the cavity. So the single quantum dot is modeled as three-level system with a ground and two excited states (A and B).

The lifetime of state B is too short to be resolved in the experiment, which gives rise to nonvanishing values in the short-time limit $t \to 0$. Such a feature is not reproducible if we assume just a single excited state A. For weaker temporal resolution, we obtain the experimental data depicted by black dots. The shortest time resolved is t = 5 ns, where both the dashed orange and the solid blue curve are almost identical. So, one may assume that additional excited states can be neglected in the experiment. We will demonstrate that the presence of the additional state B can be inferred nevertheless by accumulating the information contained in the photon statistics at all available time spans. Thereby, we will also elaborate on the required time resolution and find a remarkable high critical value of 37 ns.

EXTENDED JAYNES−CUMMINGS MODEL

Full Description. We study a plasmonic cavity hosting a single quantum dot. The system is described by the extended Jaynes−Cummings Hamiltonian

$$H_{\mathrm{exJC}} = \omega_c a^\dagger a + \sum_{i=\mathrm{A,B}} [\omega_i \sigma_i^+ \sigma_i^- + g_i(a\sigma_i^+ + a^\dagger \sigma_i^-)] \tag{1}$$

where we set $\hbar$ = 1 as we do throughout this paper. A diagram of the involved states is depicted in Figure 2a. The first term describes a single-mode cavity where the operator $a^\dagger$ (a) creates (annihilates) a boson at energy ω_c. The dot is modeled as three-level system with a ground $|\mathrm{g}\rangle$ and two excited states $|\mathrm{e_{A/B}}\rangle$. The lowering and raising operator are $\sigma_i^- = |\mathrm{g}\rangle\langle \mathrm{e}_i|$ and $\sigma_i^+ = |\mathrm{e}_i\rangle\langle \mathrm{g}|$. Jaynes−Cummings constants g_i characterize the coupling strengths between the cavity and three-level system. The form of the coupling term requires that the rotation wave approximation holds.[67,68] So, we assume that $\omega_i + \omega_c$ is much larger than all other system parameters, in contrast to $\omega_i - \omega_c$.

The dynamics of the system are determined by a master equation

$$\dot{\rho} = \mathcal{L}\rho = -i[H_{\mathrm{exJC}}, \rho] + \mathcal{D}\rho \tag{2}$$

The first term describes the unitary evolution of the system. The dissipator

$$\mathcal{D} = \kappa \mathcal{D}_a + \sum_{i=\mathrm{A,B}} (\gamma_{i\mathrm{g}} \mathcal{D}_{\sigma_i^+} + \gamma_{\mathrm{g}i} \mathcal{D}_{\sigma_i^-} + \gamma_{ii} \mathcal{D}_{\sigma_i^+\sigma_i^-} + \gamma_{\bar{i}i} \mathcal{D}_{\sigma_{\bar{i}}^+\sigma_i^-}) \tag{3}$$

accounts for incoherent dynamics. The Lindblad operator reads $\mathcal{D}_x\rho = x\rho x^\dagger - \frac{1}{2}\{x^\dagger x, \rho\}$. Population transfer from the exciton i = A, B to $\bar{i}$ = B, A is modeled by $\gamma_{\bar{i}i}\mathcal{D}_{\sigma_{\bar{i}}^+\sigma_i^-}$ and most

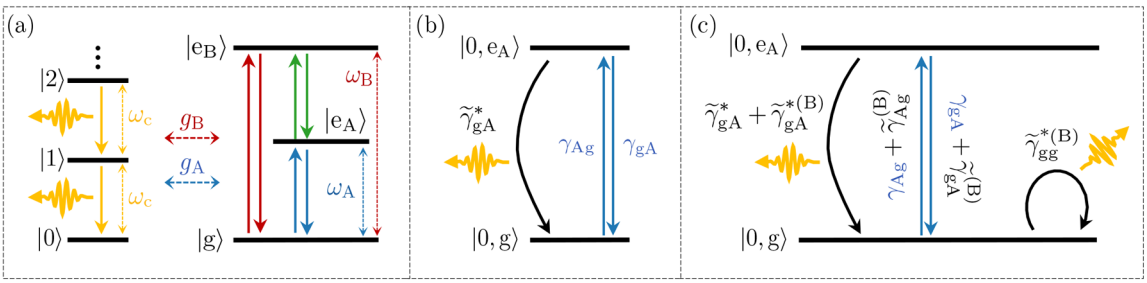

Figure 2. Extended Jaynes−Cummings model: a single-mode cavity coupled to a quantum dot with a ground and two excited states A and B. Incoherent transitions are depicted by solid arrows. (a) Full energy diagram. (b, c) Effective incoherent model applicable if the cavity field, the excited state B, and coherences decay quickly. The state B is neglected in (b).

https://doi.org/10.1021/acsphotonics.2c00375
ACS Photonics XXXX, XXX, XXX−XXX

likely due to phonon-mediated processes.[69] Dephasing is taken into account by $\gamma_{ii}\mathcal{D}_{\sigma_i^+\sigma_i^-}$. The term $\gamma_{ig}\mathcal{D}_{\sigma^+}$ describes incoherent pumping. It accounts for pumping of the quantum-dot states via another higher-energy state that is directly excited by an incident monochromatic laser followed by dephasing. The term $\kappa\mathcal{D}_a$ and $\gamma_{gi}\mathcal{D}_{\sigma_i^-}$ describe the intrinsic decay of an excitation in the cavity and quantum dot, respectively.[70] The quantum yield of the two kinds of dot excitons outside the cavity is quite different.[66] So, we can assume a bright and a dark exciton. The intrinsic decay of the latter one is most likely due to heat emission.

Effective Description. In this paper, we concentrate on the experimentally relevant parameter regime

$$\gamma_{ig} < \gamma_{gi}, \gamma_{i\bar{i}} \lesssim \Delta t^{-1} \ll g_A \ll g_B, \omega_i, \omega_c, \gamma_{ii}, \kappa \tag{4}$$

where the state B has only a weak impact on the waiting-time distribution and the second-order correlation function for times $t > 5$ ns, as illustrated in Figure 1. The photon stream is sampled at the finite time resolution Δt. So, the dynamics determined by g_i, ω_i, ω_c, γ_{ii}, and κ are too fast to be resolved in real time. We can eliminate adiabatically the corresponding degrees of freedom, which lead to effective corrections for the slower dynamics. The details of the derivation are presented in the Supporting Information, I. We use the stationary condition[71] to remove the fast degrees of freedom, that is, coherent superpositions, the cavity field as well as the excited state B (due to the strong coupling g_B). We obtain an effective incoherent kinetic rate equation for the states $|0, g\rangle$ and $|0, e_A\rangle$, where $|0\rangle$ is the vacuum state of the cavity. Momentary transient excitations lead to effective incoherent transitions rates $\tilde{\gamma}_{ji}$ between these states, where i is the initial and j the final state.

If we neglect the state B completely, we obtain the dynamics illustrated in Figure 2b. Pumping of the ground state leads to the excited state A at rate γ_{Ag}. The decay of state A at rate γ_{gA} is enhanced by the cavity-induced correction $\tilde{\gamma}^*_{gA}$, which is well-known as the Purcell effect.[70]

If we take the adiabatic corrections from state B into account, we obtain the effective dynamics illustrated in Figure 2c. The excitation rate, the intrinsic decay, and the Purcell enhancement change by $\tilde{\gamma}^{(B)}_{Ag}$, $\tilde{\gamma}^{(B)}_{gA}$, and $\tilde{\gamma}^{*(B)}_{gA}$, respectively. Moreover, the strong coupling g_B leads to the formation of two polaritonic states. However, once populated, the polaritons decay immediately on time scales that can not be resolved in the experiment. The total process of slow excitation and immediate decay can be modeled by the single rate $\tilde{\gamma}^{*(B)}_{gg} \approx \gamma_{Bg}$, as illustrated by the self-loop in Figure 2c. This process persists even in the nonresonant case $\omega_B \neq \omega_c$, if $(\omega_B - \omega_c)^2 \lesssim g_B^2(\gamma_{BB} + \kappa)/(\gamma_{AB} + \gamma_{gB})$ (see Supporting Information, I).

In conclusion, the additional state B gives rise to Poissonian photon statistics as long as the system is in its ground state. Such a statistical feature can not be generated in the framework of an ordinary Jaynes–Cummings model with just the single excited state A. We will discuss in the following sections how this contribution to the total photon emission can be identified from the photon-counting statistics.

PHOTON STATISTICS

The photon-counting statistics can be characterized by correlation functions[1,2]

$$g^{(m)}(t_1, \cdots t_m) = \frac{\langle a^\dagger(t_1)\cdots a^\dagger(t_m)a(t_m)\cdots a(t_1)\rangle}{\langle a^\dagger(t_1)a(t_1)\rangle^m} \tag{5}$$

of order m, with $t_1 < t_2 < \cdots < t_m$. They can be calculated from the Liovillian as explained in the Supporting Information, II.B. The correlation functions at zero time delay are related to the occupation number n of the cavity. A seminal expression used frequently is[2]

$$\langle n^{(m)}\rangle = \langle n\rangle^m g^{(m)}(0) \tag{6}$$

with the factorial power $n^{(m)} = n(n-1)\cdots(n-m+1)$. Correlation functions at nonzero time delay have previously received less attention in literature. They are related to the number N of counted photons during a time interval $[0, t]$. We find for the corresponding factorial moments (Supporting Information, II)

$$\langle N^{(m)}\rangle(t) = m! I_{ph}^m \int_0^t \int_{t_1}^t \cdots \int_{t_{m-1}}^t g^{(m)}(t_1, \cdots t_m)\mathrm{d}t_m \cdots \mathrm{d}t_1 \tag{7}$$

The mean photon current $I_{ph} = \langle N\rangle/t = \kappa\langle n\rangle$ is related to the cavity loss rate κ and the mean occupation number $\langle n\rangle$ of the cavity mode. From a theory perspective, these moments can be derived conveniently as derivatives $\langle N^{(m)}\rangle = \partial_z^m \mathcal{M}(z, t)|_{z=1}$ of a generating function[72] (Supporting Information, II.A):

$$\mathcal{M}(z, t) = \mathrm{Tr}[e^{\mathcal{L}_z t}\rho_{NESS}] \tag{8}$$

The Liouvillian $\mathcal{L}_z = \mathcal{L}_0 + z\mathcal{J}$ with the counting variable z characterizes the system dynamics completely and, thereby, distinguishes between a part increasing the photon counter $\mathcal{J}\rho = \kappa a\rho a^\dagger$ and a part ($\mathcal{L}_0 = \mathcal{L} - \mathcal{J}$) leaving the counter unchanged. The Liouvillian determining the time evolution of the density matrix is recovered as $\mathcal{L} = \mathcal{L}_1$. The system is subjected to constant pumping and we assume that counting starts when the nonequilibrium steady state ρ_{NESS} has been reached which fulfills $\mathcal{L}_1\rho_{NESS} = 0$. For the extended Jaynes–Cummings model depicted in Figure 2c, the effective Liouvillian (derived in the Supporting Information, I) takes the form

$$\mathcal{L}_z = \begin{pmatrix} (z-1)\tilde{\gamma}^{*(B)}_{gg} - \gamma_{Ag} - \tilde{\gamma}^{(B)}_{Ag} & z(\tilde{\gamma}^*_{gA} + \tilde{\gamma}^{*(B)}_{gA}) + \gamma_{gA} + \tilde{\gamma}^{(B)}_{gA} \\ \gamma_{Ag} + \tilde{\gamma}^{(B)}_{Ag} & -\tilde{\gamma}^*_{gA} - \tilde{\gamma}^{*(B)}_{gA} - \gamma_{gA} - \tilde{\gamma}^{(B)}_{gA} \end{pmatrix} \tag{9}$$

in the basis $(\rho_{|0,g\rangle}, \rho_{|0,e_A\rangle})^T$.

The generating function defined in eq 8 can be simplified in the limit of long time intervals t. It takes on the large deviation form $\mathcal{M}(z, t) \propto e^{\lambda_{max}(z)t}$.[73] Here, $\lambda_{max}(z)$ is the eigenvalue of the Liouvillian with the largest real part. This motivates the definition of factorial cumulants $C_{F,m}(t) = \partial_z^m \ln \mathcal{M}(z, t)|_{z=1}$ which are related to the moments via the recursive formula

$$C_{F,m}(t) = \langle N^{(m)}\rangle(t) + \sum_{i=1}^{m-1}\binom{m-1}{i-1} C_{F,i}(t)\langle N^{(m-i)}\rangle(t) \tag{10}$$

https://doi.org/10.1021/acsphotonics.2c00375
ACS Photonics XXXX, XXX, XXX–XXX

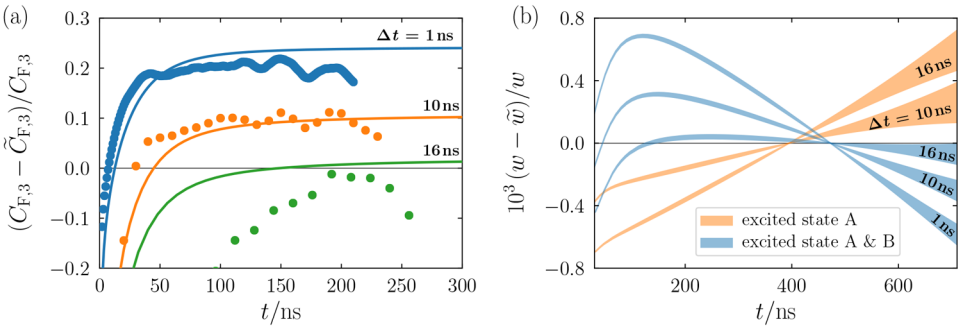

Figure 3. Testing for the presence of an additional state B using (a) the third factorial cumulant and (b) the waiting-time distribution at different sampling times Δt. The criteria given in eqs 20 and 21 are evaluated. In the long-time limit, a positive sign in (a) and a negative sign in (b) indicate the state B. A sampling time faster than 17 ns is required. Dots in (a) are measured in the experiment, whereas solid curves are simulations. Continuous error bars in (b) are simulated assuming that the photon stream is recorded for 100 s with $\eta = 1$. Other parameters are given in Methods.

and give access to the different derivatives of the dominating eigenvalue

$$\partial_z^m \lambda_{\max}(z)|_{z=1} = \lim_{t\to\infty} \frac{C_{F,m}(t)}{t} \tag{11}$$

This information can be used to reconstruct the characteristic polynomial of an unknown Liouvillian, a scheme dubbed inverse counting statistics.[74,75] The Liouvillian of the extended Jaynes−Cummings model given in eq 9 has a characteristic polynomial of the form

$$\chi(z, \lambda) = \lambda^2 + (a_{01} + a_{11}z)\lambda + a_{00} + a_{10}z \tag{12}$$

with the coefficients related to the system parameters by

$$a_{11} = -\widetilde{\gamma}_{gg}^{*(B)} \tag{13a}$$

$$a_{01} = \gamma_{Ag} + \widetilde{\gamma}_{Ag}^{(B)} + \widetilde{\gamma}_{gA}^{*} + \widetilde{\gamma}_{gA}^{*(B)} + \gamma_{gA} + \widetilde{\gamma}_{gA}^{(B)} \tag{13b}$$

$$a_{00} = (\gamma_{gA} + \widetilde{\gamma}_{gA}^{(B)})\widetilde{\gamma}_{gg}^{*(B)} + (\widetilde{\gamma}_{gA}^{*} + \widetilde{\gamma}_{gA}^{*(B)})(\gamma_{Ag} + \widetilde{\gamma}_{Ag}^{(B)} + \widetilde{\gamma}_{gg}^{*(B)}) \tag{13c}$$

Moreover, we have $a_{10} = -a_{00}$ since the existence of a nonequilibrium steady state demands that $\lambda = 0$ is an eigenvalue for $z = 1$.

The coefficients can be obtained from measured cumulants. We take advantage of eq 11, which allows us to express the derivatives $\partial_z^m \chi(z, \lambda_{\max}(z))_{z=1} = 0$ as a function of the coefficients and measured cumulants. The first three derivatives form a set of linear equations that we solve for the coefficients. As a result, we obtain

$$a_{11} = \lim_{t\to\infty}\left(\frac{3C_{F,2}^2 C_{F,1}}{(2C_{F,3}C_{F,1} - 3C_{F,2}^2)t} - \frac{C_{F,1}}{t}\right) \tag{14}$$

and similar expressions for a_{01} and a_{00}. The coefficients a_{01} and a_{00} depend on the dynamics of both excited states A and B. In contrast, a_{11} depends only on the rate $\widetilde{\gamma}_{gg}^{*(B)}$, which vanishes in the absence of the excited state B. Setting the left-hand side of eq 14 to zero, we find an asymptotic condition that must be fulfilled for the third cumulant

$$\widetilde{C}_{F,3} = \frac{3C_{F,2}^2}{C_{F,1}} \tag{15}$$

in the long-time limit.

Violation of this relation indicates the presence of the state B. We have modified the symbol of the third cumulant by a tilde $\widetilde{C}_3$ to indicate that the expression holds in general only for two state kinetics. We emphasize that the factorial cumulants can be expressed by the $g^{(m)}$ correlation functions, as shown in the Supporting Information, II.D; therefore, eq 15 is a relation between the correlation functions. Moreover, the extended James−Cummings model determined by the effective Liouvillian in eq 15 is a renewal system which is in its ground state after a photon is detected. Thus, the third-order correlation function takes the factorized form $g^{(3)}(t_1, t_2, t_3) = g^{(2)}(t_2 - t_1)\, g^{(2)}(t_3 - t_2)$, and only $g^{(2)}$ is required to evaluate eq 15.

WAITING-TIME DISTRIBUTION

A quantity providing complementary information to the correlation functions is the waiting-time distribution $w(t)$.[36−48] It is the probability density that two consecutive photons are detected at the time difference t. The distribution can be expressed as $w(t) = \langle\tau\rangle\partial_t^2 P_0(t)$, where $\langle\tau\rangle = 1/I_{ph}$ is the mean waiting time and $P_0 = \mathcal{M}(0, t)$ is the idle-time probability that no photons have been counted during the time span $[0, t]$.[76]

The idle-time probability is related to the dominating eigenvalue by $\lambda_{\max}(0) = \lim_{t\to\infty}[\ln P_0(t)]/t$. Therefore, we have an additional relation to obtain the coefficients of the characteristic polynomial. We solve the set of linear equations $\chi(z, \lambda_{\max}(z))_{z=0} = 0$, $\partial_z\chi(z, \lambda_{\max}(z))_{z=1} = 0$, and $\partial_z^2\chi(z, \lambda_{\max}(z))_{z=1} = 0$, which leads to

$$a_{11} = \lim_{t\to\infty}\left(\frac{C_{F,2}(\ln P_0)^2 - 2C_{F,1}^2 \ln P_0 - 2C_{F,1}^3}{(C_{F,2}\ln P_0 + 2C_{F,1}\ln P_0 + 2C_{F,1}^2)t}\right) \tag{16}$$

If the state B is absent and a_{11} vanishes, we obtain the condition

$$\widetilde{P}_0 = \exp\left[\frac{C_{F,1}^2}{C_{F,2}}\left(1 - \sqrt{1 + 2\frac{C_{F,2}}{C_{F,1}}}\right)\right] \tag{17}$$

and for the waiting-time distribution

$$\widetilde{w} = \langle\tau\rangle\widetilde{P}_0\left(\frac{\ln \widetilde{P}_0}{t}\right)^2 \tag{18}$$

https://doi.org/10.1021/acsphotonics.2c00375
ACS Photonics XXXX, XXX, XXX−XXX

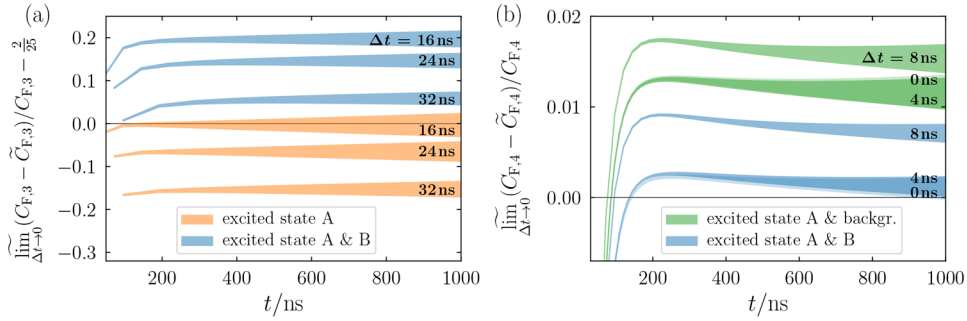

Figure 4. Testing for the presence of an additional state B using (a) the third and (b) fourth factorial cumulant while compensating for the finite sampling time Δt during photon detection, that is, the limit $\Delta t \to 0$ is approximated by a Newton series evaluating the data at Δt, $2\Delta t$, and $3\Delta t$. Continuous error bars for the expressions given in eqs 22 and 24 are depicted. (a) The state B yields a positive sign for $\Delta t < 37$ ns. (b) A vanishing value in the long time limit indicates state B for $\Delta t < 5$ ns, whereas background photons yield a nonvanishing value. We assumed that the photon stream is recorded for 500 s in (a) and for 10^7s in (b) with $\eta = 1$. Other parameters are given in Methods.

in the long-time limit. Detecting a violation of the relations in eqs 15 and 18 is a sensitive way to identify the presence of the state B. However, one must ensure that the violation is not caused by measurement imperfections, which we discuss in detail in the following sections.

PHOTON DETECTION

Single-photon detection is always subjected to experimental limitations. Intensity losses lead to a finite probability η that an emitted photon is detected. Moreover, the continuous photon stream is sampled at a finite time resolution Δt, which leads to a discrete time signal of $t/\Delta t$ points. The original generating function given in eq 8 must be adjusted accordingly

$$\mathcal{M}(z,t) = \mathrm{Tr}\left(\left\{\sum_{i=0}^{\infty}\frac{\Delta t^i}{i!}[\eta\mathcal{L}_z + (1-\eta)\mathcal{L}_1]^i_{z^n\to z}\right\}^{t/\Delta t}\rho_{\mathrm{NESS}}\right) \tag{19}$$

During the sampling time Δt, a maximum of one photon can be detected. If more photons reach the detector (counting factor z^n, with $n > 1$), the detector counter increases only by one (counting factor z). In our experimental setup, emitted photons pass a 50/50 beam splitter before being focused on two single-photon detectors, each recording its own time trace. So, two photons can be detected during each time interval $[t - \Delta t/2, t + \Delta t/2]$. In our simulations (single-detector setup, eq 19), we set $\Delta t \to \Delta t/2$ to allow for the detection of two photons during these time intervals. Similarly, the numeric values for Δt given in the following must be divided by a factor of 2 to reproduce the results in experiment by a single-detector setup.

Naturally, the relations given in eqs 15 and 18 do not hold exactly due to the modified generating function. The relative deviation from the predicted behavior of the third factorial cumulant (eq 15) is illustrated in Figure 3a for the sampling times $\Delta t = 1$, 10, and 16 ns. Simulations by means of eq 19 are depicted by solid curves and experimental data by dots. The parameters are given in the caption and the Methods section.

If we neglect state B, the relative deviations in the long-time limit take the form

$$\frac{C_{\mathrm{F},3} - \widetilde{C}_{\mathrm{F},3}}{C_{\mathrm{F},3}} = 1 - \frac{3(\Delta t'^2 - 2e^{-\Delta t'} + 2)^2}{2\Delta t'^2(\Delta t'^2 + 6)} < 0 \tag{20}$$

with $\Delta t' = (\gamma_{\mathrm{gA}} + \widetilde{\gamma}^*_{\mathrm{gA}})\Delta t$. In general, the relative deviation is nonvanishing. However, its sign is fixed, irrespective of the system or detector parameters. Therefore, an opposite sign reveals that the dynamics can not be modeled just by a single excited state. Unfortunately, the presence of the additional state B does not guarantee a different sign (Supporting Information, III). The sampling time Δt must be smaller than a certain critical value, which for the parameters used in Figure 3 is about 17 ns. Otherwise, the state B can not be resolved anymore.

The criterion given in eq 20 and the $g^{(2)}$-correlation function do not depend on the detection probability η of the emitted photons, that is, no systematic error is introduced. Decreasing the detection probability in the experiment leads only to more statistical noise, which can be compensated by increasing the measurement time and acquiring more data. In contrast, the waiting-time distribution is much more affected by a finite detection probability. We present simulations of the relative deviation from eq 18 in Figure 3b. We assume that the photon stream is recorded for 100 s, which yields the depicted continuous error bars[77] (Supporting Information, IV). In the long time limit, the deviations take the form

$$\frac{w - \widetilde{w}}{w} = -t\frac{(\Delta t'^2 + 6)(\eta\gamma_{\mathrm{Ag}}\widetilde{\gamma}^*_{\mathrm{gA}})^3}{3(\gamma_{\mathrm{gA}} + \widetilde{\gamma}^*_{\mathrm{gA}})^5}\frac{C_{\mathrm{F},3} - \widetilde{C}_{\mathrm{F},3}}{C_{\mathrm{F},3}} > 0 \tag{21}$$

Again, a different sign indicates the presence of state B. However, deviations decrease with η^3. Thus, a small detection probability makes it much more challenging to identify a certain sign in case of statistical noise due to a limited amount of data.

To surpass the time resolution limit, we suggest the following procedure, which comes at the cost of low statistical noise. First, the recorded discrete-time signal is downsampled by a factor of 2 and 3. We obtain photon streams at sampling time $2\Delta t$ and $3\Delta t$. Then, we evaluate the relative error $(C_{\mathrm{F},3} - \widetilde{C}_{\mathrm{F},3})/C_{\mathrm{F},3}$ for each stream separately. We assume that the error caused by the finite time resolution can be expanded in a Newton series around $2\Delta t$. The expansion has the form $f(x) = f(2\Delta t) + f'(2\Delta t)(x - 2\Delta t) + \frac{f''(2\Delta t)}{2}(x - 2\Delta t)^2$, with $f'(2\Delta t) = [f(3\Delta t) - f(\Delta t)]/(2\Delta t)$ and $f''(2\Delta t) = [f(3\Delta t) - 2f(2\Delta t) + f(\Delta t)]/\Delta t^2$. From this expansion we can approximate the result that would be obtainable for vanishing sampling time. Finally, the criterion in eq 20 takes the modified form

https://doi.org/10.1021/acsphotonics.2c00375
ACS Photonics XXXX, XXX, XXX−XXX

Table 1. System Parameters Used for the Different Simulations

system	$\hbar\gamma_{Ag}$ (neV)	$\hbar\gamma_{Bg}$ (neV)	$\hbar\gamma_{gA}$ (neV)	$\hbar\gamma_{gB}$ (neV)	$\hbar\gamma^0_{AB}$ (neV)	$\hbar/\Delta t$ (neV)	$\hbar g_A$ (μeV)	$\hbar g_B$ (eV)	$\hbar\omega_c$ (eV)	$\hbar\omega_A$ (eV)	$\hbar\omega_B$ (eV)	$\hbar\gamma_{AA}$ (eV)	$\hbar\gamma_{BB}$ (eV)	$\hbar\kappa$ (eV)	$\hbar\gamma_{noise}$ (neV)
excited state A	5.0		32.5			40–600	88.0		1.93	1.95		0.05		0.40	
excited state A and B	5.0	1.1	32.5	100	100	40–600	20.0	0.10	1.93	1.95	2.00	0.05	0.13	0.40	
excited state A and background	5.0		32.5			40–600	47.0		1.93	1.95		0.05		0.40	0.5

$$\lim_{\Delta t\to 0}\left(\frac{C_{F,3}-\widetilde{C}_{F,3}}{C_{F,3}}\right)<\frac{2}{25} \tag{22}$$

with $\lim_{\Delta t\to 0} f(\Delta t) := 3f(\Delta t) - 3f(2\Delta t) + f(3\Delta t)$. The maximal value of the error is 2/25, irrespective of the system and detector parameters. This is a consequence of eq 20 depending only on the effective sampling time $\Delta t'$. The criterion in eq 22 is illustrated in Figure 4a. The critical sampling time has increased significantly to 37 ns.

Processing the waiting-time distribution in a similar manner is not practical. The limit $\lim_{\Delta t\to 0}(w-\widetilde{w})/w$ scales with $(\eta\gamma_{Ag}\widetilde{\gamma}^*_{gA})^3/(\gamma_{gA}+\widetilde{\gamma}^*_{gA})^5$ and, thus, has no universal bound. The scaling factor must be known if we want to identify the presence of state B.

BACKGROUND PHOTONS

Measurements of photon statistics suffer from background photons, which lead to false detector counts. The resulting statistical features are similar to those generated by the case of an additional state B. Especially, the second-order correlation function is nonvanishing in the short-time limit.[78] However, higher-order correctors can be used to identify qualitative differences.

We incorporate the background photons in our simulation as state-independent contribution to the Liouvillian $\mathcal{L}_z + (z-1)\gamma_{noise}\mathbf{1}$. False counts are occurring at the rate γ_{noise}. Then, the characteristic polynomial given in eq 12 acquires the additional coefficient a_{20}. If the state B is present and the background can be neglected, the coefficient a_{20} vanishes and we find that the fourth factorial cumulant fulfills

$$\widetilde{C}_{F,4}=\frac{4}{3}\frac{C^2_{F,3}}{C_{F,2}}+2\frac{C_{F,3}C_{F,2}}{C_{F,1}}-3\frac{C^3_{F,2}}{C^2_{F,1}} \tag{23}$$

in the long-time limit. The details of the derivation are presented in the Supporting Information, V. The relative deviation from eq 18 does not have a universal sign for arbitrary system parameters. Therefore, we have to inspect deviations from zero which requires the measurement errors to be negligible. The error induced by the finite detection probability η is suppressed at least by a factor $O(\Delta t^4)$. To compensate for the leading orders in Δt, we suggest to analyze the criterion

$$\lim_{\Delta t\to 0}\left(\frac{C_{F,4}-\widetilde{C}_{F,4}}{C_{F,4}}\right)=0 \tag{24}$$

which holds in the absence of a photon background and for small sampling times. We illustrate the criterion in Figure 4b. The critical sampling time is 5 ns. For smaller sampling times, the finite value reveals the presence of background noise.

CONCLUSIONS

We have proposed a new procedure to analyze the information contained in the higher-order correlation functions $g^{(m)}$ at nonzero time delay. By integrating out time dependences in $g^{(m)}$, we obtain factorial cumulants, which give access to features in the photon statistics beyond the generic interpretation schemes of photon correlation functions at zero time delay.

Instead of assuming a specific stochastic model and comparing simulated with measured factorial cumulants, the procedure deals with the opposite problem: if only a few factorial cumulants are given, what can we learn about the underlying stochastic model? As output of the procedure, we obtain sign criteria whose violations exclude certain candidates for the underlying model. The sign criteria are robust against a limited counting efficiency and time resolution in experiment, that is, information can be obtained even in case that $g^{(m)}$ is not known at short times. Moreover, it can be used to evaluate the waiting-time distribution, which is known to be an information source complementary to correlation functions.

We have demonstrated the procedure for the photon emission of a plasmonic cavity coupled to a quantum dot. We have derived a criterion whose violation indicates that the underlying model is not the ordinary Jaynes–Cummings model. The violation can be explained by modeling the quantum dot as three level system or by including background photons. We have derived a criterion allowing one to distinguishing between both cases.

METHODS

Experimental Setup. Silver bowtie cavities were prepared as discussed in ref 66. In brief, bowtie cavities were made on SiN grids using electron-beam lithography followed by electron beam silver evaporation and liftoff. Semiconductor quantum dots (CdSe/ZnS) were inserted into the cavities using the capillary force method.[66] Second-order correlation measurements were performed using a MircoTime 200 (PicoQuant) single-particle spectrometer with a 488 nm laser.

Model Parameters. The simulations presented in this paper can be obtained either from the full or the effective description introduced in Extended Jaynes–Cummings Model. The model parameters for the full description are given in Table 1 and guided by ref 66. We assume that population transfer from state A to state B and vice versa is thermally activated such that

$$\gamma_{AB}=[1+f_B(\hbar\omega_B-\hbar\omega_A,T)]\gamma^0_{AB} \tag{25}$$

$$\gamma_{BA}=f_B(\hbar\omega_B-\hbar\omega_A,T)\gamma^0_{AB} \tag{26}$$

where $f_B(E,T)$ is the Bose–Einstein distribution at temperature T (we assume T = 300 K) and energy E.

https://doi.org/10.1021/acsphotonics.2c00375
ACS Photonics XXXX, XXX, XXX–XXX

We obtain the parameters for the effective description from Table 1 following the derivation shown in the Supporting Information, I. We obtain $\gamma_{Ag} + \tilde{\gamma}_{Ag}^{(B)} = 5.0$ neV and $\gamma_{gA} + \tilde{\gamma}_{gA}^{(B)} = 32.5$ neV. If state B and background photons are neglected, we get $\tilde{\gamma}_{gA}^{*} = 68.3$ neV. Taking state B into account yields $\tilde{\gamma}_{gA}^{*} + \tilde{\gamma}_{gA}^{*(B)} = 19.3$ neV and $\tilde{\gamma}_{gg}^{*(B)} = 1.1$ neV. If state B is neglected but significant background photons are taken into account, see Figure 4b, we have $\tilde{\gamma}_{gA}^{*} = 19.3$ neV and $\gamma_{noise} = 0.5$ neV.

■ ASSOCIATED CONTENT

Supporting Information

The Supporting Information is available free of charge at https://pubs.acs.org/doi/10.1021/acsphotonics.2c00375.

Derivation of the effective Liouvillian; Relations between factorial moments, factorial cumulants, and $g^{(m)}$ correlation functions; Analytic expressions for eqs 20 and 21 in case of an additional state B or background photons; Details on the calculation of continuous error bars; Inverse counting statistics in case of a general two-state model (PDF)

■ AUTHOR INFORMATION

Corresponding Author

Philipp Stegmann − *Department of Chemistry, Massachusetts Institute of Technology, Cambridge, Massachusetts 02139, United States;* orcid.org/0000-0003-4859-2095; Email: psteg@mit.edu

Authors

Satyendra Nath Gupta − *Department of Chemical and Biological Physics, Weizmann Institute of Science, Rehovot 761001, Israel; Physical Research Laboratory, Ahmedabad 380009, India*

Gilad Haran − *Department of Chemical and Biological Physics, Weizmann Institute of Science, Rehovot 761001, Israel;* orcid.org/0000-0003-1837-9779

Jianshu Cao − *Department of Chemistry, Massachusetts Institute of Technology, Cambridge, Massachusetts 02139, United States;* orcid.org/0000-0001-7616-7809

Complete contact information is available at: https://pubs.acs.org/10.1021/acsphotonics.2c00375

Notes

The authors declare no competing financial interest.

■ ACKNOWLEDGMENTS

We thank E. Kleinherbers for useful discussions. This work was supported by the NSF (CHE 1800301 and 1836913) and the School of Science fund (Sloan Fund) at MIT. P.S. acknowledges support from the German National Academy of Sciences Leopoldina (Grant No. LPDS 2019-10). Part of the work was completed during J. Cao's visit to the Weizmann Institute of Science under the sponsorship of the Rosi and Max Varon visiting Professorship.

■ REFERENCES

(1) Glauber, R. J. The Quantum Theory of Optical Coherence. *Phys. Rev.* **1963**, *130*, 2529.

(2) Loudon, R. *The Quantum Theory of Light*, 3rd ed.; Oxford Science Publications, 2000.

(3) Kondakci, H. E.; Szameit, A.; Abouraddy, A. F.; Christodoulides, D. N.; Saleh, B. E. A. Sub-thermal to super-thermal light statistics from a disordered lattice via deterministic control of excitation symmetry. *Optica* **2016**, *3*, 477.

(4) van den Berg, T. L.; Samuelsson, P. Charge-photon transport statistics and short-time correlations in a single quantum dot−resonator system with an arbitrarily large coupling parameter. *Phys. Rev. B* **2019**, *100*, 035408.

(5) Brange, F.; Menczel, P.; Flindt, C. Photon counting statistics of a microwave cavity. *Phys. Rev. B* **2019**, *99*, 085418.

(6) Bamba, M.; Imamoğlu, A.; Carusotto, I.; Ciuti, C. Origin of strong photon antibunching in weakly nonlinear photonic molecules. *Phys. Rev. A* **2011**, *83*, 021802.

(7) Nair, G.; Zhao, J.; Bawendi, M. G. Biexciton Quantum Yield of Single Semiconductor Nanocrystals from Photon Statistics. *Nano Lett.* **2011**, *11*, 1136.

(8) Xu, C.; Vavilov, M. G. Full counting statistics of photons emitted by a double quantum dot. *Phys. Rev. B* **2013**, *88*, 195307.

(9) Vester, M.; Staut, T.; Enderlein, J.; Jung, G. Photon Antibunching in a Cyclic Chemical Reaction Scheme. *J. Phys. Chem. Lett.* **2015**, *6*, 1149.

(10) Sáez-Blázquez, R.; Feist, J.; Fernández-Domínguez, A. I.; García-Vidal, F. J. Enhancing photon correlations through plasmonic strong coupling. *Optica* **2017**, *4*, 1363.

(11) Huang, R.; Miranowicz, A.; Liao, J.-Q.; Nori, F.; Jing, H. Nonreciprocal Photon Blockade. *Phys. Rev. Lett.* **2018**, *121*, 153601.

(12) Schaeverbeke, Q.; Avriller, R.; Frederiksen, T.; Pistolesi, F. Single-Photon Emission Mediated by Single-Electron Tunneling in Plasmonic Nanojunctions. *Phys. Rev. Lett.* **2019**, *123*, 246601.

(13) Sánchez Muñoz, C.; Schlawin, F. Photon Correlation Spectroscopy as a Witness for Quantum Coherence. *Phys. Rev. Lett.* **2020**, *124*, 203601.

(14) Sýkora, J.; Kaiser, K.; Gregor, I.; Bönigk, W.; Schmalzing, G.; Enderlein, J. Exploring Fluorescence Antibunching in Solution To Determine the Stoichiometry of Molecular Complexes. *Anal. Chem.* **2007**, *79*, 4040.

(15) Chung, I.; Witkoskie, J. B.; Zimmer, J. P.; Cao, J.; Bawendi, M. G. Extracting the number of quantum dots in a microenvironment from ensemble fluorescence intensity fluctuations. *Phys. Rev. B* **2007**, *75*, 045311.

(16) Amgar, D.; Yang, G.; Tenne, R.; Oron, D. Higher-Order Photon Correlation as a Tool To Study Exciton Dynamics in Quasi-2D Nanoplatelets. *Nano Lett.* **2019**, *19*, 8741.

(17) O'Brien, J. L.; Furusawa, A.; Vučković, J. Photonic quantum technologies. *Nat. Photonics* **2009**, *3*, 687.

(18) Aharonovich, I.; Englund, D.; Toth, M. Solid-state single-photon emitters. *Nat. Photonics* **2016**, *10*, 631.

(19) Radulaski, M.; Fischer, K. A.; Lagoudakis, K. G.; Zhang, J. L.; Vučković, J. Photon blockade in two-emitter-cavity systems. *Phys. Rev. A* **2017**, *96*, 011801.

(20) You, J.-B.; Xiong, X.; Bai, P.; Zhou, Z.-K.; Ma, R.-M.; Yang, W.-L.; Lu, Y.-K.; Xiao, Y.-F.; Png, C. E.; Garcia-Vidal, F. J.; Qiu, C.-W.; Wu, L. Reconfigurable photon sources based on quantum plexcitonic systems. *Nano Lett.* **2020**, *20*, 4645.

(21) Klyshko, D. N. The nonclassical light. *Phys. Usp.* **1996**, *39*, 573.

(22) Stevens, M. J.; Glancy, S.; Nam, S. W.; Mirin, R. P. Third-order antibunching from an imperfect single-photon source. *Opt. Express* **2014**, *22*, 3244.

(23) Qi, L.; Manceau, M.; Cavanna, A.; Gumpert, F.; Carbone, L.; Vittorio, M. d.; Bramati, A.; Giacobino, E.; Lachman, L.; Filip, R.; Chekhova, M. Multiphoton nonclassical light from clusters of single-photon emitters. *New J. Phys.* **2018**, *20*, 073013.

(24) Rundquist, A.; Bajcsy, M.; Majumdar, A.; Sarmiento, T.; Fischer, K.; Lagoudakis, K. G.; Buckley, S.; Piggott, A. Y.; Vučković, J. Nonclassical higher-order photon correlations with a quantum dot strongly coupled to a photonic-crystal nanocavity. *Phys. Rev. A* **2014**, *90*, 023846.

(25) Hamsen, C.; Tolazzi, K. N.; Wilk, T.; Rempe, G. Two-Photon Blockade in an Atom-Driven Cavity QED System. *Phys. Rev. Lett.* **2017**, *118*, 133604.
(26) Bin, Q.; Lü, X.-Y.; Bin, S.-W.; Wu, Y. Two-photon blockade in a cascaded cavity-quantum-electrodynamics system. *Phys. Rev. A* **2018**, *98*, 043858.
(27) Beenakker, C. W. J.; Schomerus, H. Counting statistics of photons produced by electronic shot noise. *Phys. Rev. Lett.* **2001**, *86*, 700.
(28) Kambly, D.; Flindt, C.; Büttiker, M. Factorial cumulants reveal interactions in counting statistics. *Phys. Rev. B* **2011**, *83*, 075432.
(29) Stegmann, P.; Sothmann, B.; Hucht, A.; König, J. Detection of interactions via generalized factorial cumulants in systems in and out of equilibrium. *Phys. Rev. B* **2015**, *92*, 155413.
(30) Stegmann, P.; König, J. Short-time counting statistics of charge transfer in Coulomb-blockade systems. *Phys. Rev. B* **2016**, *94*, 125433.
(31) Carmichael, H. J.; Singh, S.; Vyas, R.; Rice, P. R. Photoelectron waiting times and atomic state reduction in resonance fluorescence. *Phys. Rev. A* **1989**, *39*, 1200.
(32) Cao, J.; Silbey, R. J. Generic schemes for single-molecule kinetics. 1: Self-consistent pathway solutions for renewal processes. *J. Phys. Chem. B* **2008**, *112*, 12867.
(33) Vyas, R.; Singh, S. Photon-counting statistics of the degenerate optical parametric oscillator. *Phys. Rev. A* **1989**, *40*, 5147.
(34) Verberk, R.; Orrit, M. Photon statistics in the fluorescence of single molecules and nanocrystals: Correlation functions versus distributions of on- and off-times. *J. Chem. Phys.* **2003**, *119*, 2214.
(35) Delteil, A.; Gao, W.-b.; Fallahi, P.; Miguel-Sanchez, J.; Imamoğlu, A. Observation of Quantum Jumps of a Single Quantum Dot Spin Using Submicrosecond Single-Shot Optical Readout. *Phys. Rev. Lett.* **2014**, *112*, 116802.
(36) Zhang, X. H. H.; Baranger, H. U. Quantum interference and complex photon statistics in waveguide QED. *Phys. Rev. A* **2018**, *97*, 023813.
(37) Avriller, R.; Schaeverbeke, Q.; Frederiksen, T.; Pistolesi, F. Photon-emission statistics induced by electron tunneling in plasmonic nanojunctions. *Phys. Rev. B* **2021**, *104*, L241403.
(38) Brandes, T. Waiting times and noise in single particle transport. *Ann. Phys. (Berl.)* **2008**, *17*, 477.
(39) Rajabi, L.; Pöltl, C.; Governale, M. Waiting time distributions for the transport through a quantum-dot tunnel coupled to one normal and one superconducting lead. *Phys. Rev. Lett.* **2013**, *111*, 067002.
(40) Haack, G.; Albert, M.; Flindt, C. Distributions of electron waiting times in quantum-coherent conductors. *Phys. Rev. B* **2014**, *90*, 205429.
(41) Sothmann, B. Electronic waiting-time distribution of a quantum-dot spin valve. *Phys. Rev. B* **2014**, *90*, 155315.
(42) Kosov, D. S. Waiting time distribution for electron transport in a molecular junction with electron-vibration interaction. *J. Chem. Phys.* **2017**, *146*, 074102.
(43) Engelhardt, G.; Cao, J. Tuning the Aharonov-Bohm effect with dephasing in nonequilibrium transport. *Phys. Rev. B* **2019**, *99*, 075436.
(44) Rudge, S. L.; Kosov, D. S. Counting quantum jumps: A summary and comparison of fixed-time and fluctuating-time statistics in electron transport. *J. Chem. Phys.* **2019**, *151*, 034107.
(45) Ho, N.; Emary, C. Counting statistics of dark-state transport through a carbon nanotube quantum dot. *Phys. Rev. B* **2019**, *100*, 245414.
(46) Stegmann, P.; Sothmann, B.; König, J.; Flindt, C. Electron waiting times in a strongly interacting quantum dot: Interaction effects and higher-order tunneling processes. *Phys. Rev. Lett.* **2021**, *127*, 096803.
(47) Davis, N. S.; Rudge, S. L.; Kosov, D. S. Electronic statistics on demand: Bunching, antibunching, positive, and negative correlations in a molecular spin valve. *Phys. Rev. B* **2021**, *103*, 205408.
(48) Kleinherbers, E.; Stegmann, P.; König, J. Synchronized coherent charge oscillations in coupled double quantum dots. *Phys. Rev. B* **2021**, *104*, 165304.
(49) Stegmann, P.; Gee, A.; Kemp, N. T.; König, J. Statistical analysis of spin switching in coupled spin-crossover molecules. *Phys. Rev. B* **2021**, *104*, 125431.
(50) Landi, G. T. Waiting time statistics in boundary-driven free fermion chains. *Phys. Rev. B* **2021**, *104*, 195408.
(51) Lu, H. P.; Xun, L.; Xie, X. S. Single-molecule enzymatic dynamics. *Science* **1998**, *282*, 1877.
(52) Cao, J. Event-averaged measurements of single-molecule kinetics. *Chem. Phys. Lett.* **2000**, *327*, 38.
(53) Floyd, D. L.; Harrison, S. C.; van Oijen, A. M. Analysis of kinetic intermediates in single-particle dwell-time distributions. *Biophys. J.* **2010**, *99*, 360.
(54) Avila, T. R.; Piephoff, D. E.; Cao, J. Generic schemes for single-molecule kinetics. 2: Information content of the poisson indicator. *J. Phys. Chem. B* **2017**, *121*, 7750.
(55) Piephoff, D. E.; Cao, J. Generic schemes for single-molecule kinetics. 3: Self-consistent pathway solutions for nonrenewal processes. *J. Phys. Chem. B* **2018**, *122*, 4601.
(56) Kumar, A.; Adhikari, R.; Dua, A. Transients generate memory and break hyperbolicity in stochastic enzymatic networks. *J. Chem. Phys.* **2021**, *154*, 035101.
(57) Schlather, A. E.; Large, N.; Urban, A. S.; Nordlander, P.; Halas, N. J. Near-field mediated plexcitonic coupling and giant rabi splitting in individual metallic dimers. *Nano Lett.* **2013**, *13*, 3281.
(58) Törmä, P.; Barnes, W. L. Strong coupling between surface plasmon polaritons and emitters: a review. *Rep. Prog. Phys.* **2015**, *78*, 013901.
(59) Otten, M.; Larson, J.; Min, M.; Wild, S. M.; Pelton, M.; Gray, S. K. Origins and optimization of entanglement in plasmonically coupled quantum dots. *Phys. Rev. A* **2016**, *94*, 022312.
(60) Wersäll, M.; Cuadra, J.; Antosiewicz, T. J.; Balci, S.; Shegai, T. Observation of mode splitting in photoluminescence of individual plasmonic nanoparticles strongly coupled to molecular excitons. *Nano Lett.* **2017**, *17*, 551.
(61) Hugall, J. T.; Singh, A.; van Hulst, N. F. Plasmonic Cavity Coupling. *ACS Photonics* **2018**, *5*, 43.
(62) Leng, H.; Szychowski, B.; Daniel, M.-C.; Pelton, M. Strong coupling and induced transparency at room temperature with single quantum dots and gap plasmons. *Nat. Commun.* **2018**, *9*, 4012.
(63) Yankovich, A. B.; Munkhbat, B.; Baranov, D. G.; Cuadra, J.; Olsén, E.; Lourenço-Martins, H.; Tizei, L. H. G.; Kociak, M.; Olsson, E.; Shegai, T. Visualizing spatial variations of plasmon−exciton polaritons at the nanoscale using electron microscopy. *Nano Lett.* **2019**, *19*, 8171.
(64) Pelton, M.; Storm, S. D.; Leng, H. Strong coupling of emitters to single plasmonic nanoparticles: exciton-induced transparency and Rabi splitting. *Nanoscale* **2019**, *11*, 14540.
(65) Bitton, O.; Gupta, S. N.; Houben, L.; Kvapil, M.; Křápek, V.; Šikola, T.; Haran, G. Vacuum rabi splitting of a dark plasmonic cavity mode revealed by fast electrons. *Nat. Commun.* **2020**, *11*, 487.
(66) Gupta, S. N.; Bitton, O.; Neuman, T.; Esteban, R.; Chuntonov, L.; Aizpurua, J.; Haran, G. Complex plasmon-exciton dynamics revealed through quantum dot light emission in a nanocavity. *Nat. Commun.* **2021**, *12*, 1310.
(67) Shore, B. W.; Knight, P. L. The Jaynes-Cummings Model. *J. Mod. Opt.* **1993**, *40*, 1195.
(68) Agarwal, G. S. *Quantum Optics*; Cambridge University Press: Cambridge, England, 2009.
(69) Werschler, F.; Hinz, C.; Froning, F.; Gumbsheimer, P.; Haase, J.; Negele, C.; de Roo, T.; Mecking, S.; Leitenstorfer, A.; Seletskiy, D. V. Coupling of excitons and discrete acoustic phonons in vibrationally isolated quantum emitters. *Nano Lett.* **2016**, *16*, 5861.
(70) Novotny, L.; Hecht, B. *Principles of Nano-Optics*; Cambridge University Press, 2012.
(71) Cao, J.; Silbey, R. J. Optimization of exciton trapping in energy transfer processes. *J. Phys. Chem. A* **2009**, *113*, 13825.
(72) Plenio, M. B.; Knight, P. L. The quantum-jump approach to dissipative dynamics in quantum optics. *Rev. Mod. Phys.* **1998**, *70*, 101.

https://doi.org/10.1021/acsphotonics.2c00375
ACS Photonics XXXX, XXX, XXX−XXX

(73) Touchette, H. The large deviation approach to statistical mechanics. *Phys. Rep.* **2009**, *478*, 1.
(74) Bruderer, M.; Contreras-Pulido, L. D.; Thaller, M.; Sironi, L.; Obreschkow, D.; Plenio, M. B. Inverse counting statistics for stochastic and open quantum systems: the characteristic polynomial approach. *New J. Phys.* **2014**, *16*, 033030.
(75) Stegmann, P.; König, J. Inverse counting statistics based on generalized factorial cumulants. *New J. Phys.* **2017**, *19*, 023018.
(76) Albert, M.; Haack, G.; Flindt, C.; Büttiker, M. Electron waiting times in mesoscopic conductors. *Phys. Rev. Lett.* **2012**, *108*, 186806.
(77) Kleinherbers, E.; Stegmann, P.; Kurzmann, A.; Geller, M.; Lorke, A.; König, J. Pushing the limits in real-time measurements of quantum dynamics. *Phys. Rev. Lett.* **2022**, *128*, 087701.
(78) Brouri, R.; Beveratos, A.; Poizat, J.-P.; Grangier, P. Photon antibunching in the fluorescence of individual color centers in diamond. *Opt. Lett.* **2000**, *25*, 1294.

https://doi.org/10.1021/acsphotonics.2c00375
ACS Photonics XXXX, XXX, XXX−XXX